For published typeset version see here: https://doi.org/10.1016/j.powtec.2026.122614

Cite as: Lipiejko, N. and Jones, T.J., 2026. Experimental insights into the segregation of aerated bimodal particle-gas mixtures under shear. Powder Technology, p.122614.

Experimental insights into the segregation of aerated bimodal particle-gas mixtures under shear

Natalia Lipiejko[a,*], Thomas J. Jones[a]

[a]*Lancaster Environment Centre, Lancaster University, Library Avenue, Bailrigg, Lancaster, LA1 4YQ, United Kingdom*

Abstract

Gas-particle mixtures occur in numerous geophysical phenomena and industrial processes, yet describing and understanding their flow properties remains a challenge. The difficulty in modelling granular mixtures comes from having to consider the characteristics of individual particles, properties of the aerating gas, and the complex gas-particle interactions, all of which often change both temporally and spatially. Here, we present an experimental investigation into the properties of sheared monodisperse and bimodal granular mixtures at various levels of aeration. The effects of applied shear on particle segregation were analysed. At sufficiently high air velocities, monodisperse columns exhibit bubbling fluidisation, while bimodal columns segregate into a layer of coarser glass beads overlain by a layer of smaller particles. Our experimental data indicate that applied shear can suppress the formation of bubbles and promote a homogenous non-bubbling aeration in monodisperse columns, while for the bimodal columns, shear was observed to delay and suppress segregation and the column remained in a mixed state.

Keywords: fluidised bed, sheared granular flow, segregation, bubbling fluidisation

1. Introduction

Fluidised beds are particle-gas mixtures, where the solid particles are suspended within a fluid medium, enabling the granular mixture to behave like a fluid. Understanding the behaviour of fluidised beds is crucial for numerous industrial processes, where raw materials usually come in a granular form. These processes include, for example, production of pharmaceuticals [e.g., 1, 2, 3], formulation of food products [e.g., 4, 5, 6], CO_2 capture [7, 8], and utilisation of biomass alternative fuels [e.g., 9, 10, 11]. In the natural environment, enhanced understanding of particle-gas mixtures is necessary for forecasting runout distances and hazard management of geophysical flows such as snow avalanches, debris flows, and pyroclastic density currents [e.g., 12, 13, 14, 15]. Given this widespread occurrence across a range of both industrial products and natural processes, fluidised granular beds are a major area of interest within the field of granular physics [e.g., 16, 17, 18, 19, 20, 21].

*Corresponding author

Email addresses: n.lipiejko@lancaster.ac.uk (Natalia Lipiejko), thomas.jones@lancaster.ac.uk (Thomas J. Jones)

Experimentally, fluidised beds can be generated through the introduction of air into the base of a dry granular column. When a gas flow rate is sufficiently high, the total weight of the particles is balanced by the upward drag force exerted by the gas passing through the column. The internal friction of the particles is reduced and the column becomes fluidised [22]. The specific value of the gas velocity at which the column becomes fluidised is known as the minimum fluidisation velocity, u_{mf}. At gas velocities above u_{mf}, air bubbles may form at the base of the granular column and the column may exhibit bubbling fluidisation [22, 12, 23]. Previous studies show that if the granular column is sheared whilst being fluidised, shear might suppress the bubble formation and promote homogenous, non-bubbling fluidisation [12, 24, 23].

In many scenarios both in nature and industry, a perfectly homogenous, monodisperse particle size and density distribution is unlikely. Furthermore, during the fluidisation process particle-particle collisions generate fines in a process known as attrition [25, 26, 8, 27] and generate bimodal grain size distributions [28, 29]. In these cases, when a granular mixture comprises particles of varying sizes and densities, the particles may segregate at certain gas velocities. Segregation of particles is a process wherein particles of different sizes or densities separate from the mixture, leading to a non-uniform distribution [17, 30, 21]. In bubbling fluidised columns, as the bubbles rise through the column, they carry smaller, lighter particles to the column surface. The larger, heavier particles sink down to the bottom, creating a vertical circulation of the particles in the axial direction of the column [31, 32, 30, 21]. The non-uniform distribution and heterogeneity of segregated granular columns significantly affects key properties such as the rheology and the flow patterns, which in turn impact the performance of the column in aspects such as heat transfer and chemical reactions [21]. It is therefore crucial to understand the mechanisms leading to particle segregation as well as the segregation process. Additionally, across most industrial and natural applications granular mixtures are usually dynamic phenomena, and parameters such as the shear rate can change both spatially and temporally, influencing the particle segregation process.

The motivation for this work is to investigate how particle segregation is affected by the applied shear and how particle segregation during aeration can change the flow properties of a granular column. This study presents an experimental investigation into the dynamics of aerated bimodal granular mixtures composed of spherical glass beads of different sizes. The granular mixtures are simultaneously sheared and aerated with a known gas flow rate, and shear stress is simultaneously measured. In this contribution, we present the analysis of the measured shear stress as well as qualitative analysis of the bubble formation and the segregation processes.

2. Methodology

2.1. Particle and granular mixtures characterisation

The granular material used in the experiments consisted of Ballotini glass beads of diameter: 355-500 µm and 63-90 µm (supplied by Kuhmichel Abrasiv Limited). These two size fractions are referred to by a nominal grain size as the catching sieve mesh size, 355 µm and 63 µm hereafter. For the 355 µm particles, the mean diameter and the Sauter mean diameter are $d_{50} = 450$ µm and $d_{32} = 458$ µm. For the 63 µm particles, the mean diameter and the Sauter mean diameter are $d_{50} = 68$ µm and $d_{32} = 68$ µm. Both size fractions have a narrow particle size distribution with the ratio $d_{50}/d_{32} = 0.98$ and 1.00 for 355 µm and 63 µm glass beads, respectively. The average values of sphericity are 0.93 ± 0.00 and 0.84 ± 0.07 for 355 µm and 63 µm glass beads, respectively, where a sphericity,

ϑ, value of 1 equates to a perfect sphere. The particle density is 2491 $\pm$ 3 kg m^{-3} and 2480 $\pm$ 2 kg m^{-3} for the 355 µm and the 63 µm glass beads. Detailed particle characterisation methods and raw data are provided in the supporting information. Given the particle size distribution, sphericity, and density of the 355 µm and 63 µm glass beads, both individual nominal size fractions will be considered as monodisperse, spherical, and of uniform density for further analysis. Thus, only when both are mixed they become bimodal in terms of size.

Prior to their use, the glass beads were dried for 24 hours at 100°C in a laboratory oven to remove any moisture and then left to cool for 24 hours. The fluidisation and rheometry experiments were performed using two monodisperse and four bimodal granular mixtures with an experiment input mass m of 160.00 $\pm$ 0.05 g. The monodisperse granular mixtures consisted solely of the two nominal size fractions, 355 µm and 63 µm, and will be referred to as M355 and M63 hereafter. The bimodal granular mixtures were composed of the two nominal size fractions with different small-to-large mass ratios of 50:50, 40:60, 25:75, 10:90, and will be referred to as B50, B40, B25, and B10, respectively.

2.2. Experimental apparatus

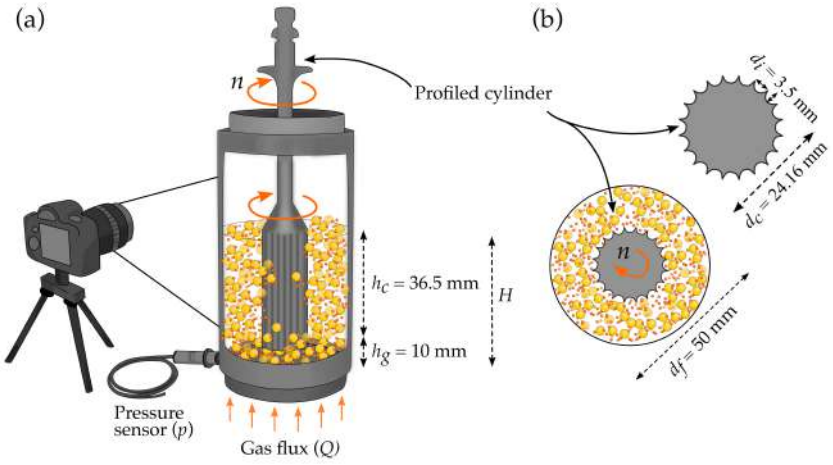

Figure 1: Diagram of the experimental apparatus modified from [23]. (a) The powder flow cell as viewed from the side; (b) The cross-section of the flow cell. Subscripts f, c, and i refer to the dimensions of the flow cell, the cylinder, and the cylinder indentations, respectively. The indentations are half-circles with a diameter of d_i. Subscript g refers to the gap set by the rheometer between the cylinder and the bottom of the flow cell.

The experiments were conducted using an Anton Paar MCR302 rheometer with a Powder Flow Cell attached (Figure 1). The Powder Flow Cell is a 50 mm in diameter cylindrical cell with a porous base connected to a compressed air supply to aerate the granular material. The inner cell walls are FTO-coated glass (Fluorine-doped Tin Oxide) to minimise the electrostatic effects. The compressed air is regulated by a Bürkert Mass Flow Controller operating at a range of 0-10 L min^{-1} for the experiments using 63 µm glass beads and all the bimodal mixtures and at a range of 0-80 L min^{-1} for the experiments using 355 µm particles. The pressure at the base of the flow cell is recorded by a Keller pressure sensor located at the bottom of the flow cell (with a measuring range of 800-2000 kPa with a maximum resolution of 0.1 kPa).

The granular material is sheared using a profiled cylinder measuring geometry that rotates at n rotations per second. The profiled cylinder is 24.16 mm in diameter with 20 evenly spaced concave indentations, which are 3.5 mm in diameter (Figure 1). The indentations extend the entire length of the cylinder, as shown in Figure 1, preventing particle slip during rotation [33]. The profiled cylinder rotating at n rotations per second shears the granular material at a shear-rate, $\dot{\gamma}$

$$\dot{\gamma} = CSR \times n, \tag{1}$$

where CSR is a Controlled shear-rate (CSR) geometry factor, typically determined by calibration with a Newtonian fluid of known viscosity [34, 35, 36]. Here, the profiled cylinder is based on ISO standard 3219 and has a CSR geometry factor of 16.392.

2.3. Experimental procedure and data collection

Bimodal granular mixtures were studied through shear stress measurements of a granular column simultaneously sheared at a constant shear-rate, $\dot{\gamma}$ and aerated with a constant air velocity, u. The experiments were performed for all the bimodal mixtures (B50, B40, B25, and B10) as well as the monodisperse mixtures (M355 and M63) for reference.

The shear stress, τ of the granular mixtures was measured at a range of gas velocities, u. To maintain a common reference point between the different columns and the measurements collected at different u, we use the apparent minimum fluidisation velocity, u_{amf}, which was determined by performing a series of pressure drop experiments. The procedure for the pressure drop experiments was as follows. The granular material was loaded into the Powder Flow Cell and mixed thoroughly with a spatula by hand to ensure a uniform particle size distribution throughout the measurement apparatus. The compressed air supply was then connected and fed into the base of the cell to aerate the glass beads. The glass beads were aerated with an increasing air flow rate, Q, from 0 L min^{-1} to Q_{max}, while the rheometer and the associated software collected the pressure data, p. The value of Q_{max} was 30, 1.5, 1.7, 1.0, 4.0, 8.0 L min^{-1} for the M355, M63, B50, B40, B25 and B10 mixture, respectively. The flow rate values were converted to air velocity using the cross-sectional area of the flow cell. The same experiments were performed with an empty Powder Flow Cell to obtain a reference value of the pressure, p_{air}, for each Q_{max}, i.e., for each granular mixture. The pressure drop across the granular column was then calculated as $\Delta p = p - p_{air}$. The apparent minimum fluidisation velocity, u_{amf} was determined from visual inspections of the pressure drop profiles produced.

The experimental procedure of the stress measurements was as follows. The granular material was loaded into the Powder Flow Cell and mixed thoroughly with a spatula by hand, again to ensure a uniform particle size distribution throughout the measurement apparatus. Although the glass beads are nearly perfectly spherical, the granular mixture was pre-sheared at $n = 1$ rps for pre-shear time $t_{ps} = 180$ s prior each measurement. This ensured that the particles have established the equilibrium orientation distributions and minimised transient oscillations in the apparent shear stress [37]. We refer the reader to Figure S3 in the supporting information which presents the stress measurements for a range of t_{ps}.

At time $t = 0$ s, the compressed air supply was turned on to aerate the glass beads with a constant flow rate of $u = 0$ u_{amf}, 0.5 u_{amf}, 1.0 u_{amf}, 1.5 u_{amf} and 2.0 u_{amf}. The granular column was also simultaneously sheared by the profiled cylinder rotating at a constant rate of n rotations per second, $n = 0.5$, 1, 3, 5, 7, 9, 13 rps, which corresponds to $\dot{\gamma} = 8$, 16, 49, 82, 115, 148, 213 s^{-1}. The

rheometer and the associated software collected the dataset, which included the shear stress, τ and the time step between the data points, dt. One hundred data points were collected, corresponding to a specific shear stress, and each individual data point was captured when the shear stress reached a stable value.

Alongside data recorded by the rheometer, additional data were also collected using an Olympus OM-D E-M10 Mark IV camera. The experiments were recorded at 2160 × 3840 pixels resolution at 30 frames per second with a 14-42 mm lens. The camera was located at the side of the rheometer and focused on the transparent flow cell window to capture the granular column. The videos were inspected visually to observe the aeration and segregation processes. Individual video frames were processed in MATLAB® to manually extract the height of the granular column, H. Having these data, the particle volume fraction, ϕ was then calculated from

$$\phi = \frac{(r_1 \times m)/\rho_1 + (r_2 \times m)/\rho_2}{A_f h_g + A_p(H - h_g)}, \tag{2}$$

where m is the mass of the granular mixture, ρ_1, ρ_2, r_1 and r_2 are the density and the percentage ratio of the 355 µm and 63 µm glass beads, respectively, A_f is the area of the base of the flow cell, A_p is the area of the ring around the profiled cylinder occupied by the particles and h_g is the gap set by the rheometer between the profiled cylinder and the base of the flow cell (Figure 1).

Individual video frames of the experiments where segregation was observed were also processed in MATLAB® to extract the temporal evolution of the thickness of the layer of 63 µm particles, h_f. These data were then analysed to determine the timescale of segregation, t_{seg}, as the time where the 63 µm layer reached its maximum thickness.

3. Results and discussion

3.1. Minimum fluidisation velocity

Figure 2 shows the pressure drop, Δp, across the granular column as a function of air velocity, u, for all the studied granular mixtures. For all the granular columns, Δp increases linearly with increasing u until it reaches a maximum value. For the monodisperse columns, after Δp reaches the maximum value, it plateaus. This occurs at the point when the weight of the column is balanced by the drag imposed by the upward gas flux and the column is fluidised. However, for the bimodal columns the behaviour is different, after Δp reaches the maximum value, it rapidly decreases and reaches a somewhat steady value. From the visual inspection of videos of the experiments, we suggest that Δp begins to decrease as the granular columns begin to segregate into separate 355 µm and 63 µm layers. The somewhat constant and steady value of Δp corresponds to the time, and hence the air velocity, when the column has reached a stable segregated state. For consistency, we determine an apparent minimum fluidisation flow rate as the value of u at which Δp reaches the maximum value for all the mixtures. The apparent minimum fluidisation velocity was thus determined to be $u_{amf} = 0.168$, 0.006, 0.004, 0.005, 0.025, 0.036 m s^{-1} for the granular mixtures M355, M63, B50, B40, B25 and B10, respectively. The experimentally determined apparent minimum fluidisation velocity will be referred to as u_{amf}, while the theoretical value and the concept of the minimum fluidisation velocity will be referred to as u_{mf} hereafter.

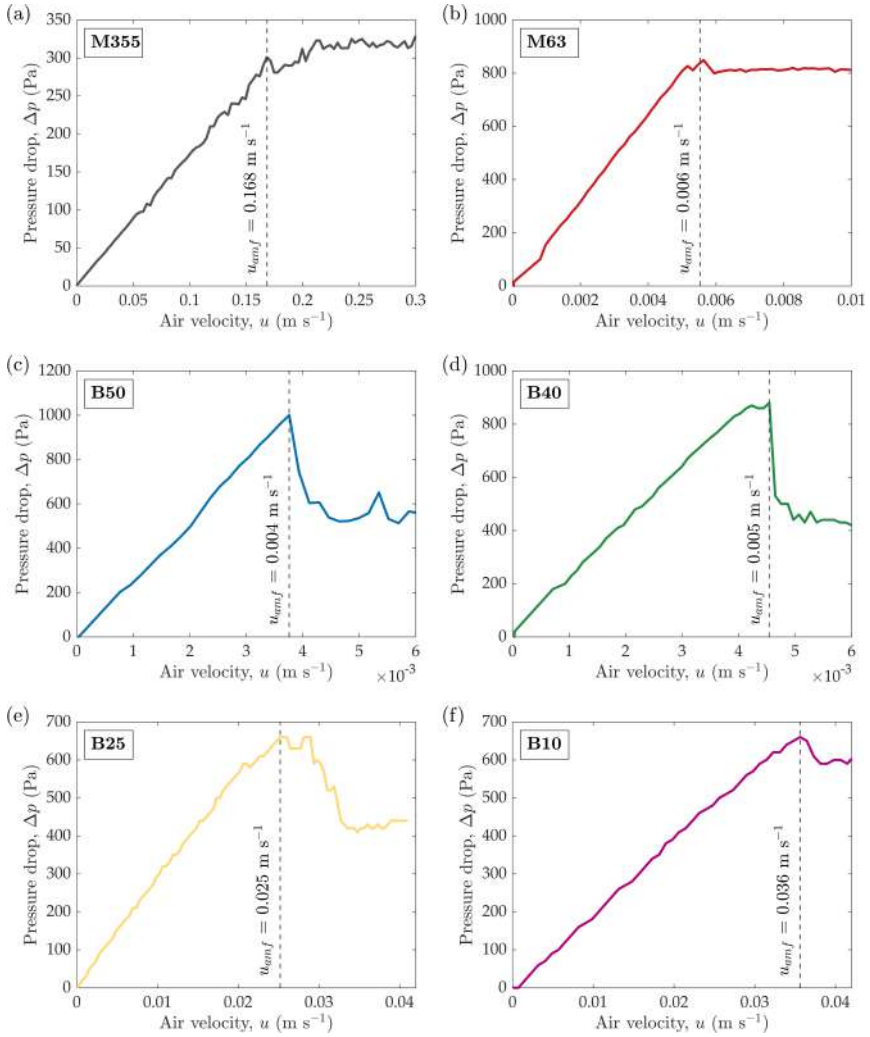

Figure 2: Pressure drop across the granular column as a function of the air flow rate under for the two monodisperse granular mixtures, (a) M355, (b) M63, and the four bimodal granular mixtures, (c) B50, (d) B40, (e) B25, (f) B10. The dashed lines represent apparent minimum fluidisation velocity, u_{amf}.

Although our method of determining u_{amf} was consistent for all the mixtures, it became apparent that there are significant challenges in determining the minimum fluidisation velocity of bimodal granular mixtures due to the large and small particles being fluidised at different velocities and hence the segregation of the granular column into separate 355 µm and 63 µm layers. Although the density ratio of the two nominal particle fractions is $\rho_1/\rho_2 \sim 1$, the size ratio is $d_1/d_2 \sim 7$, where the subscripts 1 and 2 correspond to the large and small particles, respectively. Consequently, since u_{mf} strongly depends on the particle size, the 355 µm glass beads require 30 times greater air velocities to become fluidised than the 63 µm particles, $u_{mf1}/u_{mf2} \sim 30$.

We may estimate that the value of the minimum fluidisation velocity of a bimodal mixture comprising 355 µm and 63 µm glass beads should fall between the value of minimum fluidisation velocity for 63 µm and 355 µm particles, i.e., $0.006\,\mathrm{m\ s^{-1}} = u_{mf2} < u_{mf} < u_{mf1} = 0.168\,\mathrm{m\ s^{-1}}$ [38, 21]. However, the experimentally determined values of u_{amf} for B50 and B40 are lower than u_{mf} for 63 µm, suggesting that the segregation of particles have significantly affected the pressure drop experiments and, in general, introduces uncertainties when determining u_{mf} for bimodal mixtures. As soon as the column is subjected to an air velocity greater than the minimum fluidisation velocity, the 63 µm particles move in-between the 355 µm particles and migrate towards the top of the column. It is therefore difficult to experimentally determine the exact value of u_{mf} for bimodal mixtures comprising particles of similar densities but with large size ratio.

The pressure drop method, as used here, was applied to experimentally determine the minimum fluidisation velocity of bimodal mixtures by several previous studies [e.g., 39, 40, 41, 38, 42, 20]. These data have then been used to propose semi-empirical relationships between u_{mf} and the parameters of the bimodal mixtures. For example, [20] modified the relationship by Cheung et al. [40] and put forward the equation

$$u_F = u_2\Big(\frac{u_1}{u_2}\Big)^{v^\kappa}, \tag{3}$$

with

$$v = r_1\frac{\bar{\rho}}{\rho_1}, \tag{4}$$

$$\kappa = 1.26\Big(\frac{d_1}{d_2}\Big)^{0.53}, \tag{5}$$

and the average particle density defined as

$$\frac{1}{\bar{\rho}} = \frac{r_2}{\rho_2} + \frac{r_1}{\rho_1}, \tag{6}$$

where the subscripts 1 and 2 correspond to the large and small particles, respectively. However, several authors have argued that a bimodal mixture cannot be defined with one specific value of minimum fluidisation velocity because the fluidisation takes place along an extended velocity interval with boundaries defined as the *initial*, u_{imf} and the *final fluidisation velocity* of the mixture, u_{fmf} [43, 44, 45, 21]. This theory suggests that if $u > u_{imf}$, the granular column segregates into three layers: a bottom mixed region, a layer of large particles, and a bubbling layer of small particles located at the top of the column. As the air velocity increases to $u > u_{fmf}$, the bubbles travel vertically throughout the whole column and the column becomes mixed again. Further investigation into these theories is beyond the scope of this study. Here, we use the apparent minimum fluidisation velocity simply as a reference point to relate the experiments performed using different mixtures and at different air velocities.

Alongside the u/u_{amf} ratio, each value of u corresponds to a different particle volume fraction, ϕ, which can be calculated from the image analysis of our recorded videos. This relationship is shown in Figure 3. In our experiments, for all the granular mixtures, as u increases ϕ becomes lower or equal to the initial particle volume fraction, i.e., the particle volume fraction, ϕ_0 for u

$= 0\,\mathrm{m\ s^{-1}}$. Therefore, we are confident that, in our experiments, all the granular mixtures are in different states of aeration for different u/u_{amf}. These results also highlight that a particle volume fraction, in particular, in relation to the initial volume fraction, should be considered when describing different fluidisation and aeration regimes. We will refer to the monodisperse columns as fluidised and to bimodal columns as aerated hereafter.

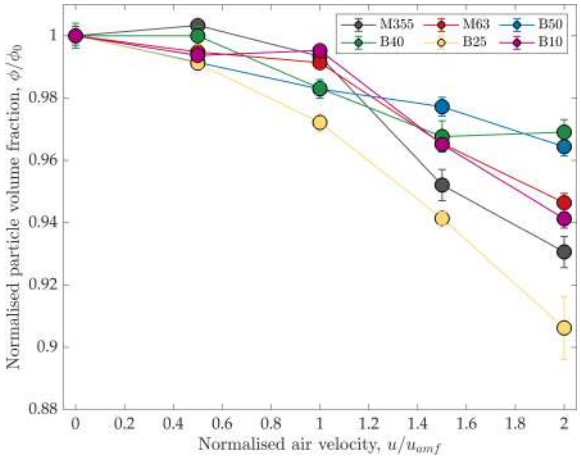

Figure 3: Normalised particle volume fraction, ϕ/ϕ_0, as a function of normalised air velocity, u/u_{amf}. The different coloured data represent different granular mixtures. The lines are not model curves and are simply used to guide the eye.

3.2. Experimental observations

When the air flow is introduced into the base of a granular column, the column starts to expand vertically and increases in height, which consequently reduces the particle volume fraction, ϕ. Column expansion is observed for all the granular columns, all the shear-rates, $\dot{\gamma}$, and all the flow rates $u > 0\,\mathrm{m\ s^{-1}}$, however it is most pronounced for $u \geq u_{amf}$. The monodisperse columns are homogeneously fluidised at $u = u_{mf}$ and experience bubbling fluidisation at $u > u_{mf}$. In bubbling fluidisation, air bubbles form at the base of the columns, move vertically upwards and most erupt, ejecting particles from the column surface. The fluidisation processes of sheared granular columns comprising monodisperse particles have been described in detail in a previous study [23]. Here, we focus on the aeration and segregation behaviour of the bimodal granular mixtures.

Figure 4 presents individual image frames of the experiments for the four bimodal granular columns, B50, B40, B25, and B10. While the specific images were chosen such that they present the most prominent processes and features, the observations are true for all the experiments performed using bimodal mixtures. When the bimodal columns are aerated with air velocities $u > 0\,\mathrm{m\ s^{-1}}$, the 63 µm glass beads (i.e., the finer particles) begin to move towards the top of the column. After a given time, the bimodal column may reach a fully segregated stable state with a coarse layer of 355 µm glass beads overlain by a thinner layer of 63 µm particles (Figures 4d and 4f). The upper layer of 63 µm particles often experiences bubbling. The 355 µm glass beads require greater air velocities to be fluidised and were only observed to experience bubbling when in the mixed state with the 63 µm particles. If the energy provided by the air velocity is not sufficient or if

it is balanced by other forces, the granular column remains in a mixed state (Figures 4a-b and 4g-h).

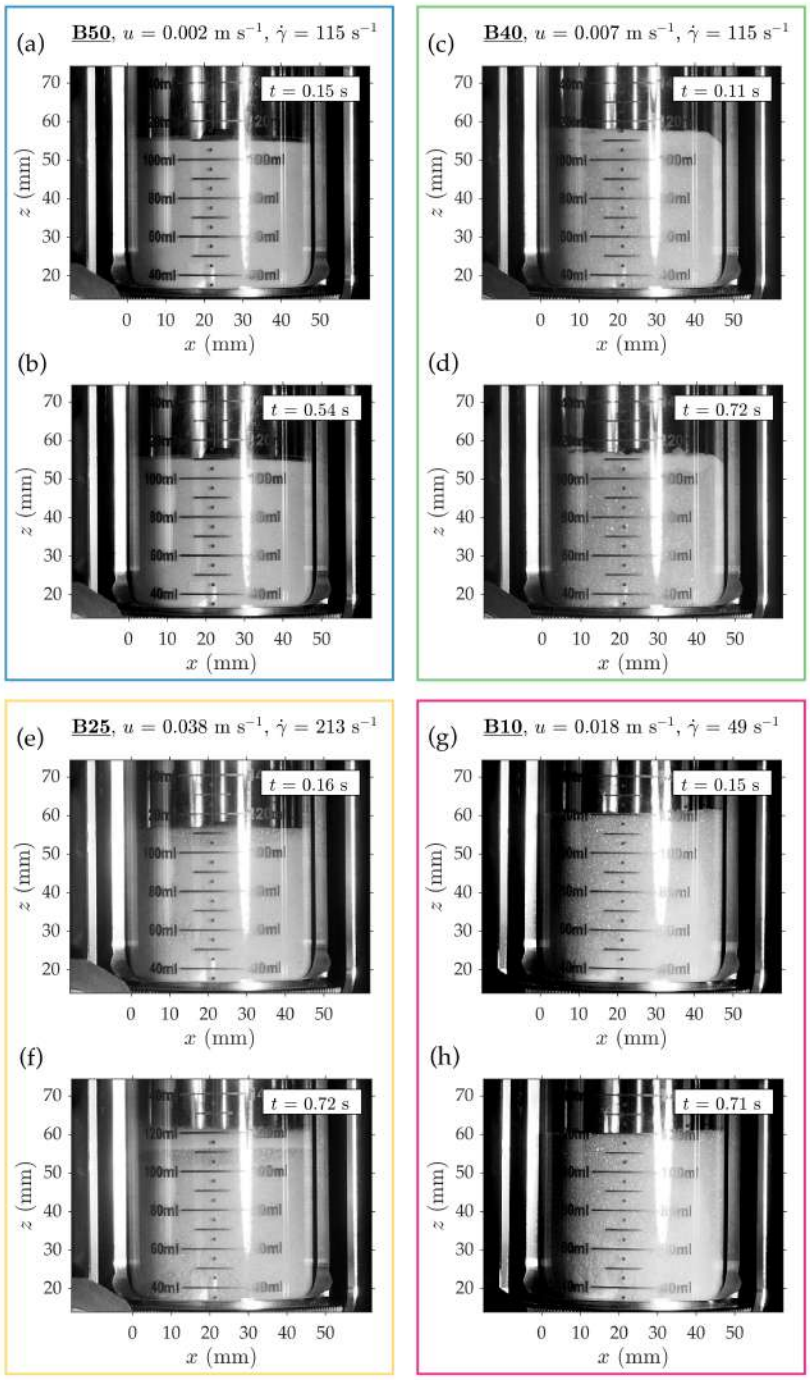

Figure 4: Individual image frames from videos of the experiments for the four bimodal columns, (a)-(b) B50, (c)-(d) B40, (e)-(f) B25, and (g)-(h) B10. The air velocity, u, and the shear-rate, $\dot{\gamma}$, is written above each experiment. The time step of each image frame is written in the top right-hand corner of each image, where $t = 0$ s is the start of the experiment. The origin of the coordinate system (x, z) is located at the bottom left corner of the flow cell.

A small number of the experiments exhibited processes such as uneven particle segregation with a preference for one side of the column and electrostatic interactions between the particles and the rheometer, causing the glass beads to stick to the flow cell and the profiled cylinder. It is possible that some of these processes were a result of heterogenous starting conditions, for example, the initial granular column was not mixed thoroughly before the start of the experiment and the particles were not evenly distributed. However, it is also possible that these processes are equipment- and experiment-specific. These experiments constitute approximately 10% of all the experiments performed using bimodal mixtures and it was not possible to process those videos to extract reliable quantitative data.

3.3. The effects of shear on column segregation

We illustrate the effects of shear on the segregation of the bimodal granular columns through image analysis of the captured videography. Figure 5 shows individual frames of the B25 granular column aerated at $u/u_{amf} = 1$ and sheared at $\dot{\gamma} = 16\,\mathrm{s}^{-1}$. Similarly, to the monodisperse granular columns, as the air velocity increases above the minimum fluidisation velocity, bubbles start to form at the base of the bimodal column and they travel vertically upwards to the column surface (Figure 5a-b). The bubbles are of different sizes and they are not necessarily spherical, as shown in Figure 5b. As the bubbles rise through the column, they carry a wake of smaller particles to the top of the column. This process can be seen in Figure 5c-d, where the green arrow indicates a bubble that travels from approximately $z = 50\,\mathrm{mm}$ to the column surface. At the surface (in Figure 5d), the breaching bubble is surrounded by a boundary composed of smaller particles. While the smaller particles ascend with the bubbles, the larger, heavier particles sink to the bottom of the column. This results in an overall circulation of particles in the axial direction of the column. The bimodal column thus begins to segregate into a layer of larger and smaller particles, a layer of 355 µm glass beads and a layer of 63 µm glass beads in our study. Given that the 63 µm glass beads are nearly seven times smaller than the 355 µm glass beads and become fluidised at much smaller air velocities, the 63 µm glass beads may also be travelling vertically upwards in the spaces between the larger particles, contributing to the segregation process. While still partly mixed, the granular column in Figure 5e shows a greater proportion of small particles in its upper layers. The bubbles are still present, indicating that the particle circulation, and hence the column segregation, is still in progress. Figure 5e shows a segregated granular column with a layer of 355 µm glass beads overlain by a layer of 63 µm glass beads. While the coarser layer is likely to still contain some proportion of small particles, the upper layer is composed of the small particles only.

The series of images in Figure 5 shows a granular column subjected to the normalised air velocity, $u/u_{amf} = 1$. As previous research suggests, it is likely that at greater air velocities both the smaller and the larger particles would fluidise and the column would remix again [43, 44, 45, 21]. In our study, some of the experiments conducted at greater air velocities exhibited electrostatic interactions between the particles and the rheometer cell walls. The glass beads stuck to the flow cell and the profiled cylinder, obstructing the view of the rest of the column. It is therefore likely that greater air velocities were sufficient to fluidise and remix both the smaller and the larger particles, but visual confirmation was obstructed.

Previous research shows that the onset of bubbling in monodisperse columns can be suppressed by applying shear to the granular column [12, 24, 23]. If the power input from shear is greater

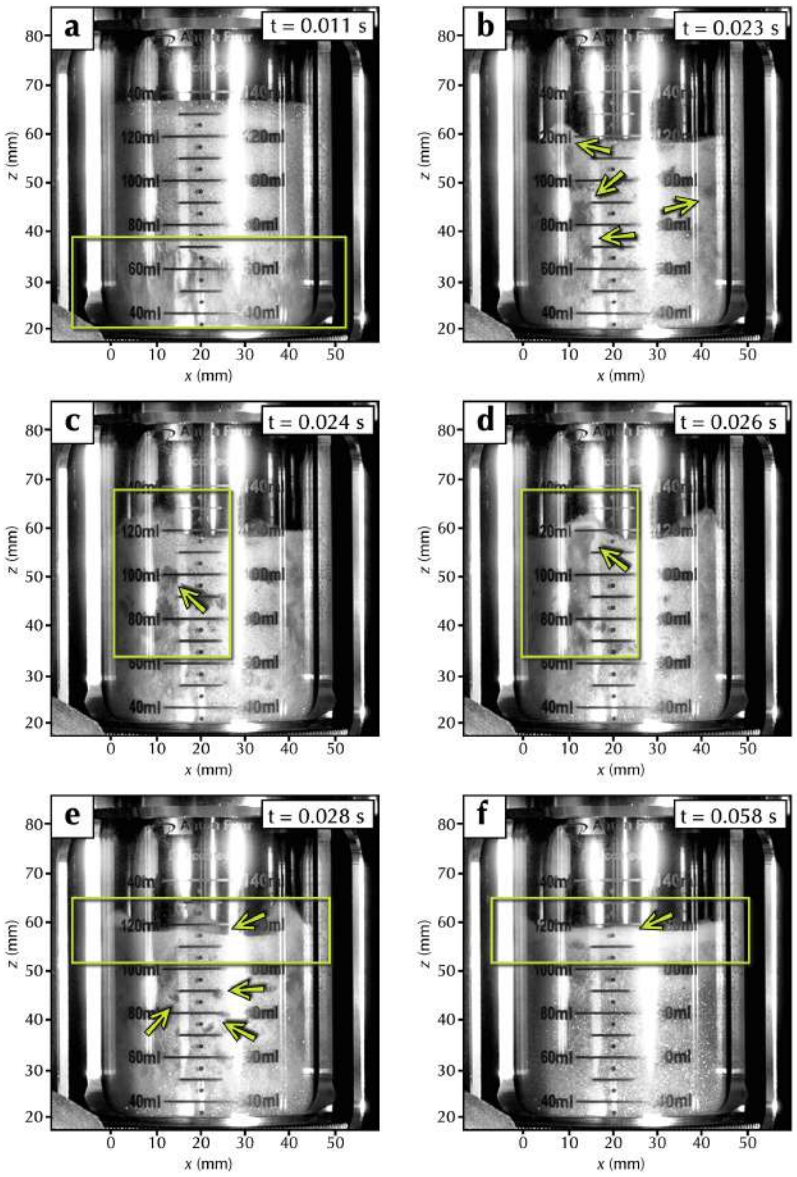

Figure 5: Individual image frames showing how the B25 granular column evolves in time (a)-(f) $t = 0.011\,\mathrm{s}$ to $0.058\,\mathrm{s}$ whilst aerated at normalised air velocity, $u/u_{amf} = 1$ and sheared at $\dot{\gamma} = 16\,\mathrm{s}^{-1}$. The origin of the coordinate system (x, z) is located at the bottom left corner of the flow cell. The green arrows and boxes point to air bubbles and other features discussed in the main text.

than the power provided by the air flow, any bubbles that may form at the base of the column are suppressed and the column remains homogenously (non-bubbling) fluidised. This indicates that there are two regimes: a fluidisation-dominated regime, where the fluidisation power is greater than

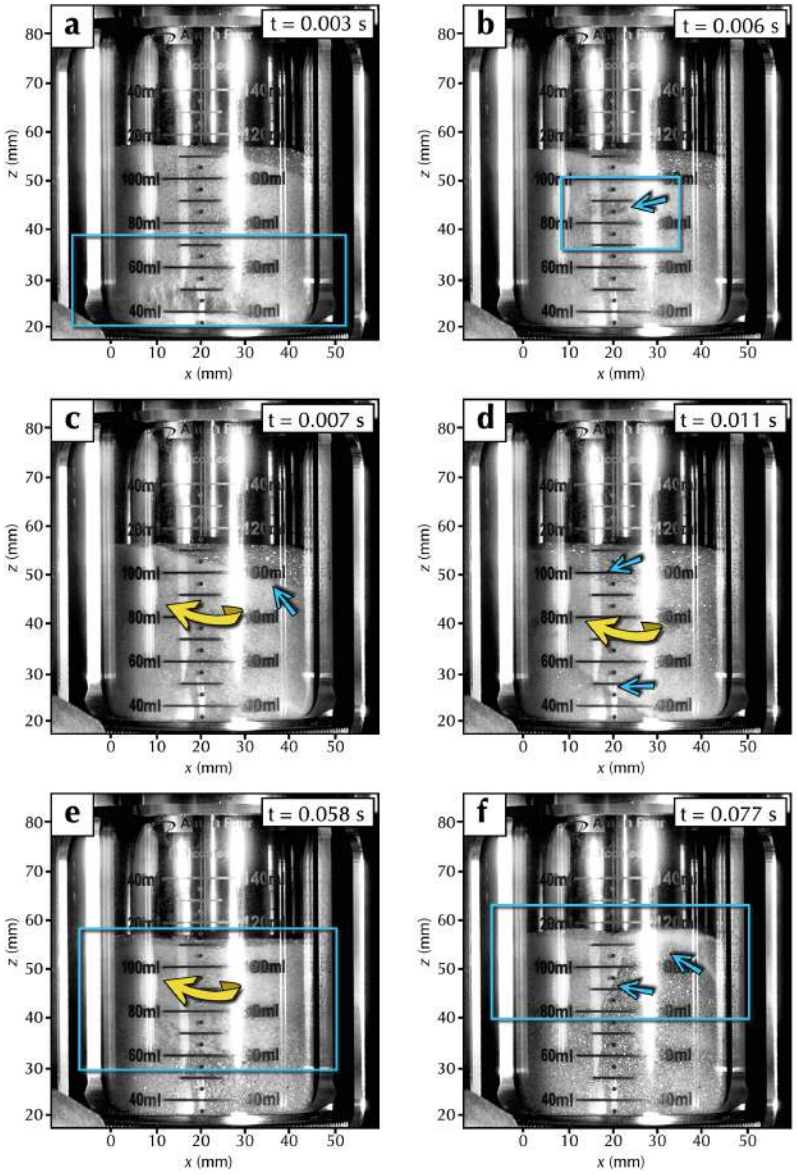

Figure 6: Individual image frames showing how the B25 granular column evolves in time (a)-(f) $t = 0.011\,\mathrm{s}$ to $0.058\,\mathrm{s}$ whilst aerated at normalised air velocity, $u/u_{amf} = 1$ and sheared at $\dot{\gamma} = 213\,\mathrm{s}^{-1}$. The origin of the coordinate system (x, z) is located at the bottom left corner of the flow cell. The yellow arrows indicate the movement of the particles and the air bubbles, while the blue arrows point to features discussed in the main text.

the shear, and a shear-dominated regime, where the shear-rate power is greater than the fluidisation input [46]. The power balance between fluidisation (aeration) and shear-rate becomes crucial in bimodal granular columns because it can indicate if a mixture will segregate at a given value of

shear-rate and air velocity.

When the air is introduced into the base of the granular column, the fluidisation power, P_D, results in an increase in the velocity of the particles. Because the column is dense (with an average particle volume fraction of $\phi \sim 0.67$), an increased particle velocity leads to increased particle-particle and particle-wall collisions, which in turn can lead to a decrease in the particle velocity. Similarly, the applied shear power, $\tau\dot{\gamma}$, can affect the velocity of the particles. The average velocity fluctuations of particles in a fluidised granular column are often quantified using the granular temperature, T [47, 48]. The power balance between fluidisation and shear can then be expressed as

$$\varrho P_D + \tau\dot{\gamma} = \varrho\Gamma\omega_c(T)T, \tag{7}$$

where ϱ is the average bulk density of the granular column, Γ is the dimensionless dissipation rate related to the coefficient of restitution and ω_c is the frequency of collisions [49, 46, 50]. The fluidisation power is usually calculated by considering the granular temperature and the collision frequency of the granular system [46], both of which depend on particle size and particle size distribution, i.e., degree of polydispersity [51, 52]. While the segregation in granular mixtures with a smaller particle size ratio than investigated here might be suppressible under very different shear rates, we suggest that the nondimensional quantities governing the power balance might be similar. Therefore, although our experimental dataset does not provide sufficient information for detailed analysis of the granular temperature, we suggest that further investigation into nondimensional quantities governing fluidisation and shear power might be key to predicting the transition point between mixed and segregated states. The power balance will now be discussed using examples from our experiments.

Figure 6 shows individual frames of the same granular column, B25, aerated with the same normalised air velocity, $u/u_{amf} = 1$, however this column now is sheared at $\dot{\gamma} = 213\,\mathrm{s}^{-1}$. Initially, we observe similar features as in Figure 5 for $\dot{\gamma} = 16\,\mathrm{s}^{-1}$. As the air velocity increases, bubbles start to form at the base of the column and they rise through the column to its surface. However, it quickly becomes apparent that the energy provided by the upward air velocity is competing with the energy input from shear. The bubbles try to carry the smaller particles to the top of the column, whilst the whole column is being sheared and rotates in the clock-wise direction, as indicated by the yellow arrows in Figure 6c-d. It appears that the vertical component of the velocity of the smaller particles increases with the rising bubbles while the radial component of the velocity depends on the applied shear. Consequently, the small particles are moving in a spiral-like pattern, as indicated by the blue arrows pointing to the edges of a wide strip of smaller particles.

Although Figure 5f and Figure 6e show the granular column at the same time, $t = 0.058\,\mathrm{s}$, there are clear differences between the two images. The granular column in Figure 5f shows a layer of larger particles and a layer of smaller particles. On the other hand, the column in Figure 6e is still rotating and in the process of segregation. More than half of this column still contains a significant proportion of small particles mixed with the large particles. A somewhat segregated column is shown in Figure 6f, where we observe a layer of large particles at the bottom and a partially mixed upper part, consisting of a mixed sublayer and a thin sublayer of small particles at the column surface.

Interestingly, the mixed sublayer is not uniformly mixed in the radial direction. Previous research shows that, particles adjacent to the profiled cylinder have a rotational velocity equal to the rotational velocity of the profiled cylinder [53]. The velocity of the particles decays in the radial plane towards the sides of the flow cell and the particles adjacent to the sides of the flow cell are nearly stationary. This leads to a heterogeneous particle volume fraction in the radial plane [53, 54, 55, 56, 23]. In bimodal granular mixtures, this may result in heterogeneities in the mixing/segregation in the radial plane. It may be easier for small particles to travel vertically upwards to the column surface in the slightly less-dense area around the profiled cylinder than for particles in the more-dense area close to the sides of the flow cell. This may be a reason for the observed rotating strip of small particles adjacent to the sides of the cell in Figure 6c-d. If the flow cell was wider, the applied shear might not be sufficient to cause the column rotation and might result in a (thick) stationary layer of particles adjacent to the sides of the cell. Conversely, particles in the area around the profiled cylinder have greater rotational velocities, which, in theory, should be able to balance the air velocities and remain in the mixed state. It is, however, important to note that all the observations are based on 2D images of 3D processes.

Nevertheless, this analysis highlights the complexity of processes governing particle segregation and illustrates that when a fluidised (aerated) granular column is subjected to shear, shear affects the internal dynamics. Analogously to previous research conducted on monodisperse granular mixtures [12, 24, 23], our experiments show that the onset of bubbling can be suppressed by applying shear to the granular column. Sheared monodisperse columns exhibit non-bubbling fluidisation over a wider range of air velocities. In this study, shear delays bubble formation in bimodal granular columns, effectively resulting in mixed-state columns over a wider range of air velocities. In general, if the power input from shear is greater than the fluidisation (aeration) power, bubble formation and hence the segregation is suppressed, and the column remains in a mixed or a partially mixed state.

3.4. Shear stress measurements: mixed and segregated states

To further investigate the effects of shear on bimodal granular columns, we analyse the shear stress data collected by the rheometer. Figure 7 presents measurements of the shear stress, τ as a function of time, t of monodisperse granular mixtures M355 and M63 for a range of shear and air flow rates. As expected, apart from very minor oscillations, the shear stress is constant in time for a constant shear-rate, for both M355 and M63 mixtures for all the studied shear-rates and air velocities. For both mixtures, the shear stress is lower when the granular columns are fluidised with greater air velocities, i.e., for lower particle volume fractions, which means that it is easier for the aerated ($u > 0\,\mathrm{m\ s^{-1}}$) granular mixtures to start flowing than for a dry, dense ($u = 0\,\mathrm{m\ s^{-1}}$) granular material. In accordance with the present results, previous studies have demonstrated that the apparent viscosity of fluidised granular mixtures decreases with the greater air velocities, enhancing the mobility of the mixture [e.g., 57, 58, 59, 60]. Similarly, since granular mixtures M355 have greater particle volume fraction than M63 mixtures, the shear stress is greater for M355 columns than for M63 when fluidised with the same normalised air velocity, u/u_{amf} and sheared at the same shear-rate, $\dot{\gamma}$. These result suggests that granular columns comprising 63 µm glass beads are more mobile than columns composed of 355 µm particles and is consistent with previous research which found that the apparent viscosity of fluidised monodisperse granular mixture increases with higher particle volume fraction [e.g., 58, 61]. Additionally, our results show that the shear stress of both mixtures depends on the applied shear-rate (compare Figure panels 7a with 7d), indicating

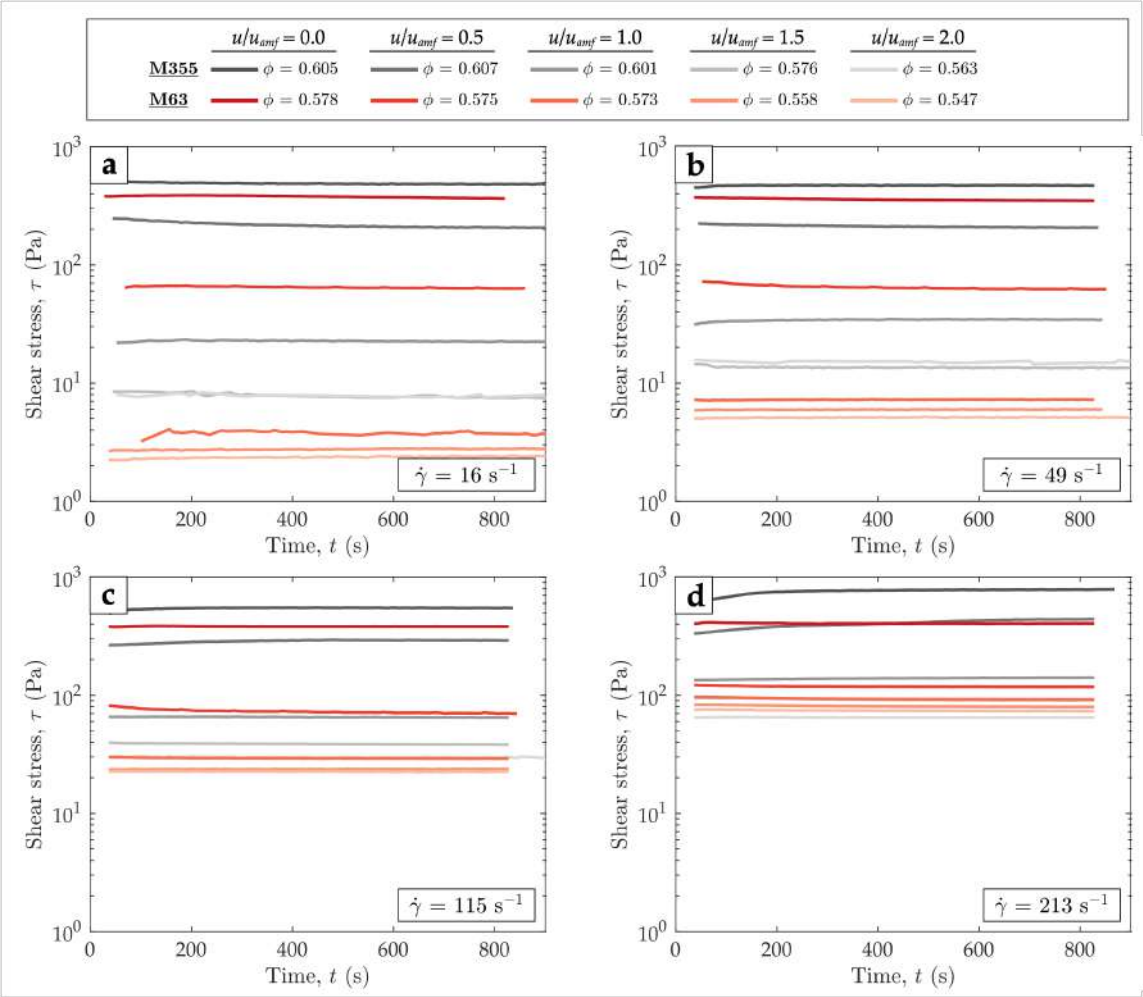

Figure 7: Shear stress, τ, of the monodispersed granular mixtures, M355 and M63, as a function of time, t, fluidised with a constant air velocity, u, and sheared at a constant rate, (a) $\dot{\gamma} = 16\,s^{-1}$, (b) $\dot{\gamma} = 49\,s^{-1}$, (c) $\dot{\gamma} = 115\,s^{-1}$, and (d) $\dot{\gamma} = 213\,s^{-1}$. The particle volume fraction, ϕ, of the granular mixtures fluidised at various air velocities is provided in the legend at the top of the figure. The y-axis, shear stress, τ, limits are the same on all panels to support cross-comparison.

non-Newtonian rheological behaviour [57, 58, 36, 33].

The measurements of τ, of the bimodal granular mixtures B50, B40, B25, and B10 for a range of air flow and shear-rates are shown in Figure 8. We distinguish three types of experiments: (i) experiments where no segregation was visually observed and the granular columns remained in a mixed state for the duration of the experiment (solid lines in Figure 8), (ii) experiments where clear segregation was observed and the column segregated into a layer of 355 µm and 63 µm glass beads (dashed lines in Figure 8), and (iii) experiments which exhibit partial, uneven, partial segregation

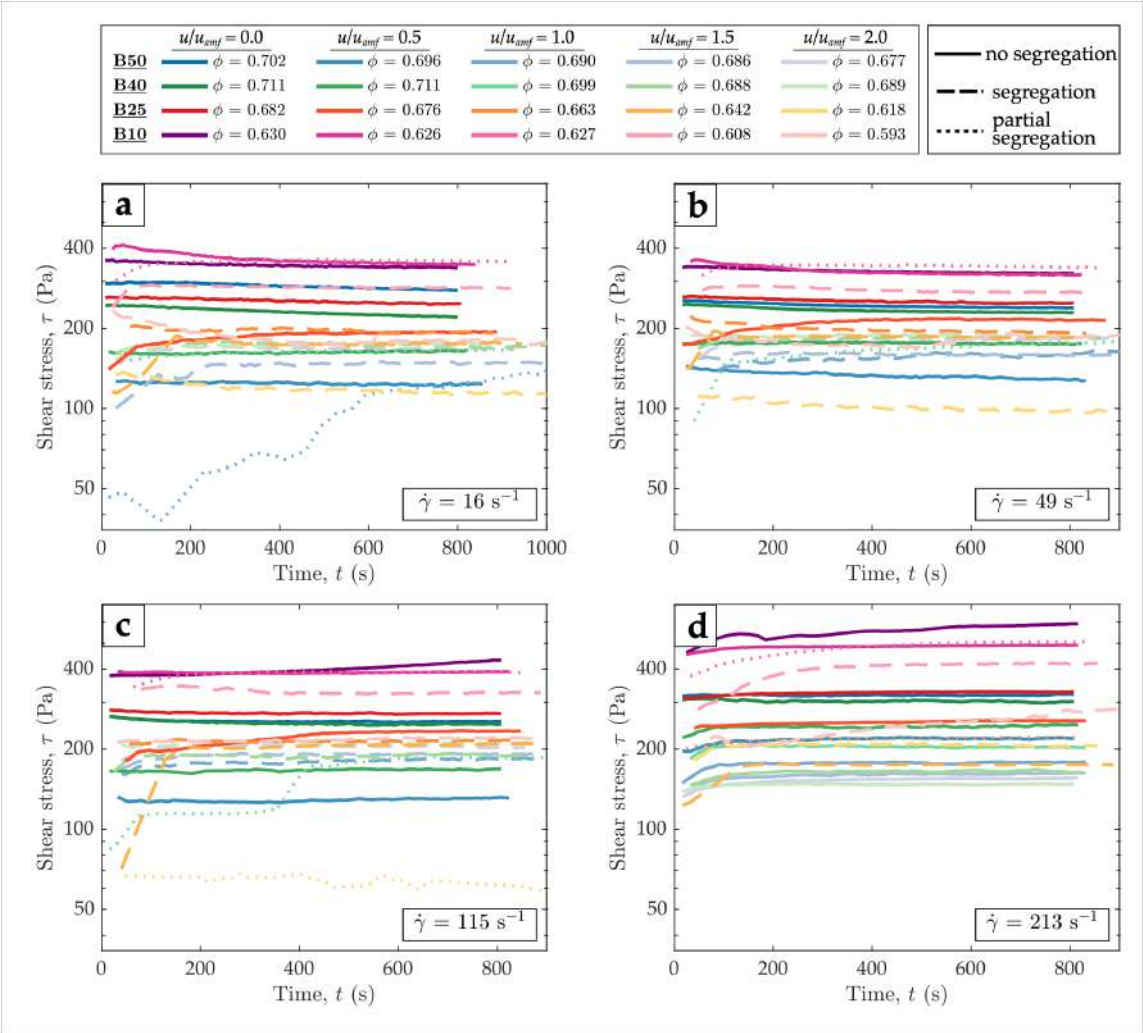

Figure 8: Shear stress, τ, of the bimodal granular mixtures, B50, B40, B25, and B10, as a function of time, t, fluidised with a constant air velocity, u, and sheared at a constant rate, (a) $\dot{\gamma} = 16\,\mathrm{s}^{-1}$, (b) $\dot{\gamma} = 49\,\mathrm{s}^{-1}$, (c) $\dot{\gamma} = 115\,\mathrm{s}^{-1}$, and (d) $\dot{\gamma} = 213\,\mathrm{s}^{-1}$. The solid lines represent experiments where no segregation was observed, the dashed lines represent experiments where segregation was clearly observed, and the dotted lines represent experiments which were discarded in further analysis. The particle volume fraction, ϕ, of the granular mixtures fluidised at various air velocities is provided in the legend at the top of the figure. The y-axis, shear stress, τ, limits are the same on all panels to support cross-comparison.

or other unusual features (dotted lines in Figure 8).

Regardless of the shear-rate applied, all the bimodal mixtures remain in the mixed state for the air velocities lower than the apparent minimum fluidisation velocity, $u < u_{amf}$. Conversely, in our experiments, whether the segregated state is observed for $u \geq u_{amf}$ depends on the applied shear-rate. The segregation process also appears to be controlled by the particle size distribution

(i.e., the degree of bimodality) because not all the bimodal mixtures achieve a segregated state for the same shear-rate and the same normalised air velocity.

Similarly to the monodisperse columns, for all the shear-rates, the shear stress of the majority of the bimodal mixtures in the mixed state is relatively constant in time. However, we observe an initial increase in shear stress for some of the mixtures, e.g., B25 mixture aerated at $u = 0.5u_{amf}$ and sheared with $\dot{\gamma} = 16$ and $49\,\mathrm{s}^{-1}$. Although all the mixtures were pre-sheared before the measurements, the initially lower shear stress values could be attributed to the particles rearranging themselves into a stable configuration state for the given shear-rate and flow rate. The timescale of this rearrangement is most likely slightly greater than the time required for initial data acquisition.

While shear stress of the bimodal mixtures in the segregated state also increases until it reaches a plateau (dashed lines in Figure 8), the timescales are longer, and these data correspond to different processes. The analysis of the data collected by the rheometer alongside the videos of the experiments indicates that here, the shear stress values reflect the evolving configuration of the granular mixture, where the particles are rearranging themselves to form a stable segregated state with 63 µm glass beads on top of 355 µm particles.

Figure 9a presents an example dataset extracted from individual video frames, specifically, the thickness of the 63 µm layer, h_f, as a function of time, t are reported. Although there are differences in the values of h_f and t between the experiments, this figure and the data pattern are representative of all the bimodal mixtures that segregated into 355 µm and 63 µm layer. As the granular column is subjected to a sufficiently high air flow h_f increases until it reaches a relatively stable maximum value at time $t = t_{seg}$. The upper 63 µm layer often exhibits bubbling, which results in fluctuations of h_f about the plateau. The values of t_{seg} for all the bimodal granular columns for a range of air velocities u and a range of shear-rates $\dot{\gamma}$ are shown in Figure 9b. The B10 columns (i.e., the bimodal columns with the smallest contributions of fine particles) appear to segregate the slowest, however, we found no clear relationship between t_{seg} and any parameters. Comparing Figure 9b with Figure 8, it is evident that the segregation time is greater than the time required for the rheometer to collect the first shear stress measurements, but it is significantly shorter than the total duration of the experiment.

The analysis of the shear stress data shows that an aerated bimodal granular mixture subjected to shear does not have the same shear stress at the beginning and at the end of the measurement. This implies that the particle distribution and hence the flow pattern of the mixture both change in time whilst undergoing aeration and shearing processes. This in turn highlights the importance of considering the applied shear when predicting the state of mixing or segregation of the mixture for designing systems relying on the different behaviour of the solid phases.

4. Conclusions

This paper reports an experimental investigation into the effects of shear on particle segregation of aerated bimodal granular columns. The columns were composed of Ballotini glass beads of nominal diameters 63 µm and 355 µm mixed in four different proportions. The granular columns made up of 50%, 40%, 25%, and 10% 63 µm by mass were compared to the results of two monodisperse columns, comprised 100% 355 µm and 100% 63 µm, respectively. The granular mixtures were

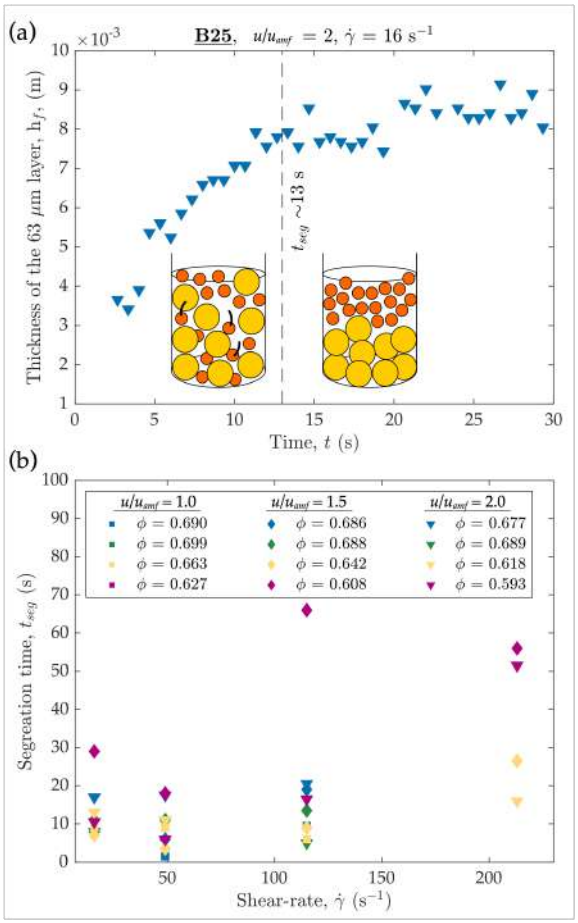

Figure 9: (a) Thickness of the upper fine layer, h_f, as a function of time, t for a bimodal mixture B25 fluidised at air velocity $u =$ m s^{-1} and sheared at $\dot{\gamma} = 16\,\mathrm{s}^{-1}$. The dashed line represents the segregation time, t_{seg}. (b) The segregation time, t_{seg}, for all the segregated bimodal granular columns for a range of air velocities, u and shear rates, $\dot{\gamma}$.

sheared at shear rates of $8\,\mathrm{s}^{-1} \leq \dot{\gamma} \leq 213\,\mathrm{s}^{-1}$ while simultaneously fluidised by a flux of compressed air at velocities 0 $u_{amf} \leq u \leq 2$ au_{mf}, where u_{amf} is the apparent minimum fluidisation velocity. Regardless of the shear-rate applied, $\dot{\gamma}$, all the granular columns expand when aerated with air velocities $u > 0\,\mathrm{m\ s}^{-1}$. At sufficiently high air velocities, air bubbles form at the base of the column and move vertically upwards towards the column surface. For monodisperse columns, the column exhibits bubbling fluidisation, while, for the bimodal columns, the 63 µm glass beads move towards the top of the column and the column segregates into a layer of 355 µm glass beads overlain by a layer of 63 µm particles. In bimodal columns, the applied shear was observed to suppress bubble formation, resulting in reduced particle segregation. Additionally, the results show that the segregation of particles affects the shear stress and hence the flow patterns of the granular mixture, therefore highlighting the the importance of considering the applied shear when predicting the state of mixing, mobility, or segregation of granular mixtures.

Acknowledgments

We would like to acknowledge the Natural Environment Research Council (NERC) who funded this research (Grant reference number: NE/W006286/1). TJJ was also supported by a UK Research and Innovation (UKRI) Future Leaders Fellowship (Grant reference number: MR/W009781/1).

Data availability statement

Data supporting the findings of this study are openly available at 10.5281/zenodo.14651636.

References

[1] W. L. Davies, W. T. Gloor Jr, Batch Production of Pharmaceutical Granulations in a Fluidized Bed I: Effects of Process Variables on Physical Properties of Final Granulation, Journal of Pharmaceutical Sciences 60 (1971) 1869–1874. doi:10.1002/jps.2600601224.

[2] P. Begat, D. A. V. Morton, J. N. Staniforth, R. Price, The Cohesive-Adhesive Balances in Dry Powder Inhaler Formulations II: Influence on Fine Particle Delivery Characteristics, Pharmaceutical Research 21 (2004) 1826–1833. doi:10.1023/B:PHAM.0000045236.60029.cb.

[3] M. W. Stocker, M. J. Harding, V. Todaro, A. M. Healy, S. Ferguson, Integrated Purification and Formulation of an Active Pharmaceutical Ingredient via Agitated Bed Crystallization and Fluidized Bed Processing, Pharmaceutics 14 (2022). doi:10.3390/pharmaceutics14051058.

[4] N. Jinapong, M. Suphantharika, P. Jamnong, Production of instant soymilk powders by ultrafiltration, spray drying and fluidized bed agglomeration, Journal of Food Engineering 84 (2008) 194–205. doi:https://doi.org/10.1016/j.jfoodeng.2007.04.032.

[5] C. Turchiuli, M. Fuchs, M. Bohin, M. E. Cuvelier, C. Ordonnaud, M. N. Peyrat-Maillard, E. Dumoulin, Oil encapsulation by spray drying and fluidised bed agglomeration, Innovative Food Science & Emerging Technologies 6 (2005) 29–35. doi:https://doi.org/10.1016/j.ifset.2004.11.005.

[6] M. J. Dev, R. G. Warke, G. M. Warke, G. B. Mahajan, R. S. Singhal, Fluidized bed granulation of gellan gum: Investigations of binder effect on physical, structural and rheological properties, Powder Technology 415 (2023) 118199. doi:https://doi.org/10.1016/j.powtec.2022.118199.

[7] Z. Sun, M. Xiao, S. Wang, D. Han, S. Song, G. Chen, Y. Meng, Sulfur-rich polymeric materials with semi-interpenetrating network structure as a novel lithium–sulfur cathode, J. Mater. Chem. A 2 (2014) 9280–9286. doi:10.1039/C4TA00779D.

[8] A. Knight, N. Ellis, J. R. Grace, C. J. Lim, CO2 sorbent attrition testing for fluidized bed systems, Powder Technology 266 (2014) 412–423. doi:https://doi.org/10.1016/j.powtec.2014.06.013.

[9] Z. Luo, H. Song, Y. Huang, B. Jin, Recent Advances on the Uses of Biomass Alternative Fuels in Cement Manufacturing Process: A Review, Energy & Fuels 38 (2024) 7454–7479. doi:10.1021/acs.energyfuels.3c04535.

[10] M. Materazzi, Gasification of Waste Derived Fuels in Fluidized Beds: Fundamental Aspects and Industrial Challenges, in: Clean Energy from Waste: Fundamental Investigations on Ashes and Tar Behaviours in a Two Stage Fluid Bed-Plasma Process for Waste Gasification, Springer International Publishing, Cham, 2017, pp. 19–63. doi:10.1007/978-3-319-46870-9_2.

[11] R. A. Cocco, J. W. Chew, Fluidized Bed Scale-Up for Sustainability Challenges. 1. Tomorrow's Tools, Industrial & Engineering Chemistry Research 63 (2024) 2519–2533. doi:10.1021/acs.iecr.3c04146.

[12] T. H. Druitt, G. Bruni, P. Lettieri, J. G. Yates, The fluidization behaviour of ignimbrite at high temperature and with mechanical agitation, Geophysical Research Letters 31 (2004). doi:10.1029/2003GL018593.

[13] G. Lube, E. C. P. Breard, S. J. Cronin, J. Jones, Synthesizing large-scale pyroclastic flows: Experimental design, scaling, and first results from PELE, Journal of Geophysical Research: Solid Earth 120 (2015) 1487–1502. doi:10.1002/2014JB011666.

[14] T. J. Jones, F. Beckett, B. Bernard, E. C. P. Breard, F. Dioguardi, J. Dufek, S. Engwell, J. Eychenne, Physical properties of pyroclastic density currents: relevance, challenges and future directions, Frontiers in Earth Science 11 (2023).

[15] N. J. Middleton, Desert dust hazards: A global review, Aeolian Research 24 (2017) 53–63. doi:https://doi.org/10.1016/j.aeolia.2016.12.001.

[16] D. Geldart, Elsevier Sequoia SA, Lausanne-Printed in the Netheriands Types of Gas Fhidization, Technical Report, 1973.

[17] A. C. Hoffmann, L. Janssen, J. Prins, Particle segregation in fluidised binary mixtures, Chemical Engineering Science 48 (1993) 1583–1592. doi:https://doi.org/10.1016/0009-2509(93)80118-A.

[18] P. Richard, M. Nicodemi, R. Delannay, P. Ribière, D. Bideau, Slow relaxation and compaction of granular systems, Nature Materials 4 (2005) 121–128. doi:10.1038/nmat1300.

[19] T. Deng, K. A. Paul, M. S. A. Bradley, L. Immins, C. Preston, J. F. Scott, E. H. Welfare, Investigations on air induced segregation of pharmaceutical powders and effect of material flow functions, Powder Technology 203 (2010) 354–358. doi:https://doi.org/10.1016/j.powtec.2010.05.028.

[20] Z. Fu, J. Zhu, S. Barghi, Y. Zhao, Z. Luo, C. Duan, Minimum fluidization velocity of binary mixtures of medium particles in the Air Dense medium fluidized bed, Chemical Engineering Science 207 (2019) 194–201. doi:10.1016/j.ces.2019.06.005.

[21] X. Zhu, X. Jiang, Y. Liu, Z. Wang, H. Wang, R. Ocone, Mixing/segregation characteristics and bubble behaviors of density-segregated binary particles in a pressurized fluidized bed, Powder Technology 434 (2024) 119367. doi:10.1016/j.powtec.2024.119367.

[22] M. Rhodes, Introduction to Particle Technology, second ed., John Wiley & Sons Ltd, Chichester, 2008.

[23] N. Lipiejko, T. J. Jones, Permeability of granular mixtures under shear, Powder Technology 444 (2024) 120064. doi:10.1016/j.powtec.2024.120064.

[24] P. Bareschino, T. Gravina, L. Lirer, A. Marzocchella, P. Petrosino, P. Salatino, Fluidization and de-aeration of pyroclastic mixtures: The influence of fines content, polydispersity and shear flow, Journal of Volcanology and Geothermal Research 164 (2007) 284–292. doi:10.1016/j.jvolgeores.2007.05.013.

[25] W. L. Forsythe, W. R. Hertwig, Attrition Characteristics of Fluid Cracking Catalysts, Industrial & Engineering Chemistry 41 (1949) 1200–1206. doi:10.1021/ie50474a015.

[26] G. Xiao, J. R. Grace, C. J. Lim, Attrition characteristics and mechanisms for limestone particles in an air-jet apparatus, Powder Technology 207 (2011) 183–191. doi:https://doi.org/10.1016/j.powtec.2010.10.028.

[27] A. Akbari, S. Y. Salehibai, Impact of Cs and Ni promotion on attrition resistance and catalytic performance of formulated spray-dried SAPO-34 in fluidized-bed MTO conversion, Powder Technology 465 (2025) 121316. doi:https://doi.org/10.1016/j.powtec.2025.121316.

[28] T. J. Jones, J. K. Russell, C. J. Lim, N. Ellis, J. R. Grace, Pumice attrition in an air-jet, Powder Technology 308 (2017) 298–305. doi:https://doi.org/10.1016/j.powtec.2016.11.051.

[29] T. J. Jones, J. K. Russell, Ash production by attrition in volcanic conduits and plumes, Scientific Reports 7 (2017) 5538. doi:10.1038/s41598-017-05450-6.

[30] M. J. Rhodes, X. S. Wang, M. Nguyen, P. Stewart, K. Liffman, Study of mixing in gas-fluidized beds using a DEM model, Chemical Engineering Science 56 (2001) 2859–2866. doi:https://doi.org/10.1016/S0009-2509(00)00524-8.

[31] R. M. Marsheck, A. Gomezplata, Particle flow patterns in a fluidized bed, AIChE Journal 11 (1965) 167–173. doi:https://doi.org/10.1002/aic.690110135.

[32] P. N. Rowe, P. BA, A. G. Cheney, G. A. Henwood, E. Lyall, Mechanisms of solids mixing in fluidised beds, Transactions of the Institution of Chemical Engineers and the Chemical Engineer 43 (1965) T271.

[33] T. Jones, A. Shetty, C. Chalk, J. Dufek, H. Gonnermann, Identifying rheological regimes within pyroclastic density currents, Nature Communications 15 (2024). doi:10.1038/s41467-024-48612-7.

[34] R. W. Whorlow, Rheological techniques, Ellis Horwood, New York, 1992.

[35] T. G. Mezger, 4th Edition, Vincentz Network, Hannover, Germany, 2012. doi:doi:10.1515/9783748600367.

[36] H. M. Mader, E. W. Llewellin, S. P. Mueller, The rheology of two-phase magmas: A review and analysis, 2013. doi:10.1016/j.jvolgeores.2013.02.014.

[37] S. Mueller, E. W. Llewellin, H. M. Mader, The rheology of suspensions of solid particles, Proceedings of the Royal Society A: Mathematical, Physical and Engineering Sciences 466 (2010) 1201–1228. doi:10.1098/rspa.2009.0445.

[38] K. Noda, S. Uchida, T. Makino, H. Kamo, Minimum fluidization velocity of binary mixture of particles with large size ratio, Powder Technology 46 (1986) 149–154. doi:10.1016/0032-5910(86)80021-3.

[39] W. R. A. Goossens, G. L. Dumont, G. L. Spaepen, Fluidization of binary mixtures in the laminar flow region, Chem. Eng. Prog. Symp. Ser. 67 (1971) 38–45.

[40] L. Cheung, A. W. Nienow, P. N. Rowe, Minimum fluidisation velocity of a binary mixture of different sized particles, Chem. Eng. Sci. 29 (1974) 1301–1303.

[41] E. Obata, H. Watanabe, N. Endo, Measurement of size and size distribution of particles by fluidization, Journal of Chemical Engineering of Japan 15 (1982) 23–28. doi:10.1252/jcej.15.23.

[42] B. Paudel, Z.-G. Feng, Prediction of minimum fluidization velocity for binary mixtures of biomass and inert particles, Powder Technology 237 (2013) 134–140. doi:https://doi.org/10.1016/j.powtec.2013.01.031.

[43] B. Formisani, R. Girimonte, T. Longo, The fluidization process of binary mixtures of solids: Development of the approach based on the fluidization velocity interval, Powder Technology 185 (2008) 97–108. doi:https://doi.org/10.1016/j.powtec.2007.10.003.

[44] B. Formisani, R. Girimonte, V. Vivacqua, Fluidization of mixtures of two solids differing in density or size, AIChE Journal 57 (2011) 2325–2333. doi:https://doi.org/10.1002/aic.12450.

[45] B. Formisani, R. Girimonte, V. Vivacqua, Fluidization of mixtures of two solids: A unified model of the transition to the fluidized state, AIChE Journal 59 (2013) 729–735. doi:https://doi.org/10.1002/aic.13876.

[46] W. T. Kranz, F. Frahsa, A. Zippelius, M. Fuchs, M. Sperl, Rheology of Inelastic Hard Spheres at Finite Density and Shear Rate, Physical Review Letters 121 (2018) 148002. doi:10.1103/PhysRevLett.121.148002.

[47] I. Goldhirsch, Introduction to granular temperature, Powder Technology 182 (2008) 130–136. doi:https://doi.org/10.1016/j.powtec.2007.12.002.

[48] D. Serero, C. Goldenberg, S. H. Noskowicz, I. Goldhirsch, The classical granular temperature and slightly beyond, Powder Technology 182 (2008) 257–271. doi:https://doi.org/10.1016/j.powtec.2007.08.002.

[49] O. R. Walton, R. L. Braun, Viscosity, granular-temperature, and stress calculations for shearing assemblies of inelastic, frictional disks, Journal of Rheology 30 (1986) 949–980. doi:10.1122/1.549893.

[50] W. T. Kranz, F. Frahsa, A. Zippelius, M. Fuchs, M. Sperl, Integration through transients for inelastic hard sphere fluids, Physical Review Fluids 5 (2020) 24305. doi:10.1103/PhysRevFluids.5.024305.

[51] S. S. Hsiau, L. S. Lu, C. H. Tai, Experimental investigations of granular temperature in vertical vibrated beds, Powder Technology 182 (2008) 202–210. doi:10.1016/j.powtec.2007.09.015.

[52] G. D. Cody, J. Johri, D. Goldfarb, Dependence of particle fluctuation velocity on gas flow, and particle diameter in gas fluidized beds for monodispersed spheres in the Geldart B and A fluidization regimes, Powder Technology 182 (2008) 146–170. doi:10.1016/j.powtec.2007.06.013.

[53] G. D. R. MiDi, On dense granular flows, The European Physical Journal E 14 (2004) 341–365. doi:10.1140/epje/i2003-10153-0.

[54] C. T. Veje, D. W. Howell, R. P. Behringer, Kinematics of a two-dimensional granular Couette experiment at the transition to shearing, Physical Review E 59 (1999) 739–745. doi:10.1103/PhysRevE.59.739.

[55] D. M. Mueth, G. F. Debregeas, G. S. Karczmar, P. J. Eng, S. R. Nagel, H. M. Jaeger, Signatures of granular microstructure in dense shear flows, Nature 406 (2000) 385–389. doi:10.1038/35019032.

[56] L. Bocquet, W. Losert, D. Schalk, T. C. Lubensky, J. P. Gollub, Granular shear flow dynamics and forces: Experiment and continuum theory, Physical Review E 65 (2001) 11307. URL: https://link.aps.org/doi/10.1103/PhysRevE.65.011307. doi:10.1103/PhysRevE.65.011307.

[57] P. Anjaneyulu, D. V. Khakhar, Rheology of a gas-fluidized bed, Powder Technology 83 (1995) 29–34. doi:https://doi.org/10.1016/0032-5910(94)02922-B.

[58] Y. Zhao, L. Wei, Rheology of gas–solid fluidized bed, Fuel Processing Technology 68 (2000) 153–160. doi:https://doi.org/10.1016/S0378-3820(00)00122-3.

[59] P. Lettieri, D. Macrì, Effect of Process Conditions on Fluidization, KONA Powder and Particle Journal 33 (2016) 86–108. doi:10.14356/kona.2016017.

[60] Y. Bai, P. Zhao, M. Guo, G. Yan, C. Zhou, Z. Sun, T. Gao, B. Zhang, Apparent viscosity of high-density fluidized bed and synergistic effect of density and apparent viscosity on particle separation, Energy Sources, Part A: Recovery, Utilization, and Environmental Effects 45 (2023) 4822–4838. doi:10.1080/15567036.2023.2205362.

[61] A. Colafigli, L. Mazzei, P. Lettieri, L. Gibilaro, Apparent viscosity measurements in a homogeneous gas-fluidized bed, Chemical Engineering Science 64 (2009) 144–152. doi:https://doi.org/10.1016/j.ces.2008.08.036.